

The best place and time to live in the Milky Way

R. Spinelli ^{*1}, G. Ghirlanda², F. Haardt^{1,2,3}, G. Ghisellini², G. Scuderi⁴

¹ Dipartimento di Scienza e Alta Tecnologia, Università dell'Insubria, Via Valleggio 11, 22100 Como, Italy

² INAF – Osservatorio Astronomico di Brera, Via E. Bianchi 46, 23807 Merate (LC), Italy

³ INFN – Sezione Milano–Bicocca, Piazza della Scienza 3, 20126 Milano, Italy

⁴ Dipartimento di Fisica G. Occhialini, Università Milano–Bicocca, Piazza della Scienza 3, 20126 Milano, Italy

Received September 18, 2020; accepted

ABSTRACT

Context. Among the most powerful cosmic events, supernovae (SNe) and γ -ray bursts (GRBs) can be highly disruptive for life: their radiation can be harmful for biota or induce extinction by removing most of the protective atmospheric ozone layer on terrestrial planets. Nearby high-energy transient astrophysical events have been proposed as possible triggers of mass extinctions on Earth.

Aims. We aim at assessing the habitability of the Milky Way (MW) along its cosmic history against potentially disruptive astrophysical transients with the scope of identifying the safest places and epochs within our Galaxy. We also test the hypothesis that long GRBs had a leading role in the late Ordovician mass extinction event (~ 440 Myrs ago).

Methods. We characterise the habitability of the MW along its cosmic history as a function of galactocentric distance of terrestrial planets. We estimate the dangerous effects of transient astrophysical events (long/short GRBs and SNe) with a model which binds their rate to the specific star formation and metallicity evolution within the Galaxy along its cosmic history. Our model also accounts for the probability of forming terrestrial planets around FGK and M stars.

Results. Until ~ 6 billion years ago the outskirts of the Galaxy were the safest places to live, despite the relatively low density of terrestrial planets. In the last ~ 4 billion years, regions between 2 and 8 kpc from the center, featuring a higher density of terrestrial planets, became the best places for a relatively safer biotic life growth. We confirm the hypothesis that one long GRB had a leading role in the late Ordovician mass extinction event. In the last 500 Myrs, the safest galactic region is comprised between 2 and 8 kpc from the center of the MW, whereas the outskirts of the Galaxy have been sterilized by 2–5 long GRBs.

Key words. Gamma-ray-burst: general, Galaxy: evolution, Astrobiology

1. Introduction

One of the primary goals of exoplanetary research is to find habitable worlds. In order to assess the very notion of "habitable" we must rely on our understanding of the reasons behind the presence/absence of lifeforms in the Solar System. Several factors determined the appearance and development of life on the planet Earth. In addition to particular intrinsic properties of the planet (e.g., geology and magnetic field) and solar characteristics (e.g., spectrum and irradiation), it is understood that a key requirement for the development of life on Earth is the presence of liquid water on the planetary surface. Indeed, potentially habitable exoplanets are identified based on their localisation within the Circumstellar Habitable Zone (CHZ - e.g., Kasting et al. 1993; Kopparapu et al. 2013).

In addition to "local" factors, planetary habitability could also be influenced by the galactic environment, for example by astrophysical events outside the solar system which can irradiate the planet. As many studies suggest (e.g., Ruderman 1974; Thorsett 1995; Dar et al. 1998; Gehrels et al. 2003; Melott & Thomas 2011; Svensmark 2012), high-energy transients such as Supernovae (SNe) and Gamma Ray Bursts (GRBs) could be life-threatening and a potential cause of mass-extinctions. A GRB, with a typical isotropic equivalent energy of 10^{52} erg located within ~ 1 kpc from the Earth, would irradiate its atmosphere with a γ -ray (i.e. keV–MeV) fluence ≥ 100 kJ m⁻² (10^8 erg cm⁻²). Such level of irradiation can produce stratospheric ni-

trogen compounds, which quickly destroy on average the 90% of the ozone layer (Thomas et al. 2005a). As a first consequence, the larger Sun UVB radiation reaching the Earth surface would result harmful to life. Intense UVB radiation could also be lethal to surface marine life such as phytoplankton, which is crucial for food chain and oxygen production. Moreover, the opacity of the NO₂ produced in the stratosphere would reduce the visible sunlight reaching the surface, causing a global cooling. As argued by Herrmann & Patzkowsky (2002) and Herrmann et al. (2003), the late Ordovician mass extinction event (~ 440 Myr ago), i.e. one of the big five mass extinctions on Earth, has some climatic signatures interpretable invoking an extra-terrestrial cause such as a nearby GRB (Melott et al. 2005).

The potentially dangerous effects of transient astrophysical events depend on their total energy released as high energy radiation, and their occurrence rate in the Galaxy: more powerful events can be lethal for a planet over larger distances, while high event rate can also reduce the ability of the planet to recover from the environmental effects induced by its radiation. Piran & Jimenez (2014) and Li & Zhang (2015) consistently find that long duration GRBs (with observed duration > 2 s - LGRBs hereafter) are the most dangerous astrophysical events for the Earth, outpacing short duration GRBs (lasting < 2 s - SGRBs hereafter) and SNe. This is mainly due to the large energy 10^{51-54} ergs (isotropic equivalent) released by LGRBs which compensates, compared to SNe, for their lower intrinsic rate ($\sim 5 \times 10^{-6}$ yr⁻¹ per galaxy according to Wanderman & Piran 2010). In particular, there is a non-negligible probability (50% according to

* email: r.spinelli@studenti.uninsubria.it

Piran & Jimenez 2014) that the Earth, in the last 500 Myr, could have been illuminated by one long lethal GRB (precisely ~ 0.93 according to Li & Zhang 2015).

The rate of astrophysical events is linked to the properties (and their variation with cosmic time) of the environment where they occur. The rate of LGRBs, being connected to the end life of massive stars (e.g., Woosley 1993), should be proportional to the efficiency of conversion of gas into stars (i.e. the star formation rate - SFR). However, their progenitors should have a low metallicity to conserve the angular momentum necessary for efficiently launching the jet (Woosley & Heger 2006; Yoon et al. 2006). This argument roughly agrees with the observed preference of long GRB for happening in relatively low metallicity host galaxies (e.g., Japelj et al. 2016; Palmerio et al. 2019). Therefore, in computing the evolution of the rate of long GRBs within the Galaxy one should account for the possible evolution of the SFR and the gas metallicity with cosmic time and within the Galaxy.

Apparently, the outer regions of the MW seems to be the most favorable for preserving life (Piran & Jimenez 2014; Li & Zhang 2015; Vukotić et al. 2016) due to the reduced SFR. However, Piran & Jimenez (2014) and Li & Zhang (2015) scaled the cosmological rate of long GRBs proportionally to the stellar mass of the MW disk, assuming constant metallicity and specific Star Formation Rate (sSFR). In this work we account for the radial distribution and the inside-out evolution of metallicity and star formation rate within the Galaxy.

The ever-increasing discovery of extrasolar planets (~ 4270 at present) motivates the extension of such studies to the whole Galaxy, accounting also for the terrestrial planet density. Gowanlock et al. (2011), Spitoni et al. (2014) and Vukotić et al. (2016) define a Galactic Habitable Zone (GHZ) by considering only SNe as possible deleterious events and focusing on terrestrial planets orbiting around FGK stars. It is worth extending these studies by considering GRBs and M dwarfs, i.e. the most powerful astrophysical events and the most abundant stellar population in the MW, respectively.

In this work we examine the astrophysical constraints for life in the MW considering, for the first time, all the most energetic transient events (short GRBs, long GRBs and SNe). We link their rates to the specific star formation within the Galaxy and to its variation with cosmic time through a semi-analytical model describing the evolution of the MW galaxy. For long GRBs we consider time the variation of the metallicity of the MW. Finally, we account for the probability of forming terrestrial planets (also dependent from the metallicity) around FGK and M stars (Zackrisson et al. 2016). We identify the astrophysically safest locations along the Milky way history, suitable for the presence of a planet with a long lasting biosphere.

Our work is organized as follows. In §2 we present the methods to estimate the number of lethal events as a function of the position within the Galaxy and of the cosmic time. In §3 we present model assumptions and the model adopted to compute the evolution of the star formation, metallicity and planetary density within the MW. In §4 and §5 we present and discuss our results. We adopt a Λ CDM cosmological model with $\Omega_M = 0.3$, $\Omega_\Lambda = 0.7$ and $H_0 = 70 \text{ km s}^{-1} \text{ Mpc}^{-1}$.

2. Methods

2.1. Cosmic Rate

For a generic population of astrophysical sources described by a function ξ in the luminosity-redshift ($L - z$) space, the cosmic

rate (number of events per unit comoving volume and time) at any cosmic epoch is:

$$\frac{dN}{dVdz} = \int_L \xi(L, z) dL \quad (1)$$

2.2. Scaling down to the Milky Way

In order to estimate the rate of a population of astrophysical sources within the MW, we rescale, at any cosmic epoch, its known cosmic rate within the cosmological volume occupied by the Galaxy:

$$\frac{dN_{\text{MW}}(z)}{dz} = \int \xi(L, z) V_{\text{MW}}(z) \mathcal{P}(z) dL \quad (2)$$

where $V_{\text{MW}}(z) = M_\star(z)/\rho_\star(z)$ is the cosmological volume occupied by MW at a given redshift, $\rho_\star(z)$ is the average stellar density as a function of redshift $\rho_\star(z) = 10^{17.46-0.39z} \text{ M}_\odot \text{ Gpc}^{-3}$ (Li & Zhang 2015; Mortlock et al. 2015) and $M_\star(z)$ is the stellar mass of the evolving Milky Way (§3.5). $\mathcal{P}(z)$ is the probability of occurrence of astrophysical sources (i.e. LGRB, SGRB, SN) within the MW at a given cosmic epoch (the cosmic time is here represented as the redshift z). This probability depends from the cosmic evolution of the MW properties (e.g. specific star formation rate and metallicity in the case of LGRBs) which can inhibit or favor the occurrence of the lethal transient sources under consideration.

2.3. Rate of lethal events within the MW

The fluence produced by astrophysical transients on a planetary atmosphere is the primary ingredient leading to possible lethal effects. Thomas et al. (2005a,b) estimated, through a 2-D atmospheric model, that a γ -ray fluence of 10 kJ m^{-2} can induce on average a 68% depletion of the ozone layer at an altitude of 32 km on a time scale of a month. Larger fluences, i.e. 100 kJ m^{-2} and 1000 kJ m^{-2} would produce depletions up to 91% and 98% respectively. We consider a depletion of 91% of the ozone layer enough to produce mass extinctions (see also Thomas et al. 2005a,b; Li & Zhang 2015). Therefore, we define astrophysical "lethal events" those capable to illuminate a planetary atmosphere with a fluence (i.e. energy flux integrated over the event's duration) $F \geq 100 \text{ kJ/m}^2$ (i.e. 10^8 erg cm^2 , F_c).

Given a population of astrophysical events the lethal effect on a planet can be quantified by computing the rate of lethal events. At any cosmic time, the rate per unit time of lethal events (i.e with a fluence $\geq F_c$) for a planet at distance R from the Galactic center is:

$$\frac{dN_{\text{MW}}(R, z)}{dz} = \int \xi(L, z) V_{\text{MW}}(z) \mathcal{P}(d, z|R) dL \quad (3)$$

where $\mathcal{P}(d, z | R)$ (see §2.4) is the portion of Galaxy which is dangerous (i.e. the fraction of the MW within a distance d from R) and describes the probability of occurrence of lethal events (i.e with energy and distance producing a fluence $\geq F_c$) within the MW given its local properties. The integral is performed over the entire luminosity distribution.

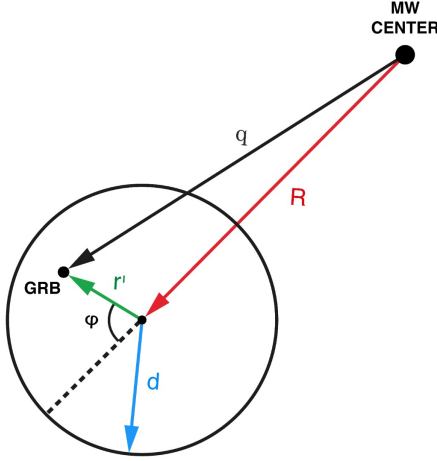


Fig. 1. Portion of galaxy potentially dangerous (solid black circle). The hazard distance d identifies the circular region within which a GRB of energy $E \geq 4\pi d^2 F_c$ can produce a lethal fluence. q represents the galactocentric distance of the GRB. In this sketch the center of the polar coordinate system (identified by the arrow R) is where the planet lies.

2.4. Dangerous portion of Galaxy

We define the hazard distance $d(L, F_c)$ of an astrophysical event with energy E as the (lethal) distance within which its fluence is higher than F_c :

$$d(L, F_c) = \sqrt{\frac{E}{4\pi F_c}} \quad (4)$$

Assuming that GRBs and SNe follow the stellar distribution within the Milky Way, $\mathcal{P}(d, z | R)$ at a given time t , can be calculated by integrating the MW stellar surface density $\Sigma_*(R, z)$ (see §3.5) within a distance d from the planet position (R):

$$\mathcal{P}(d, z | R) = \frac{1}{M_*(z)} \int_S \Sigma_*(R, z) da \quad (5)$$

We adopt a polar coordinate system (see Fig. 1), centered at the position at distance R from the Galaxy center, to calculate $\mathcal{P}(d, z | R)$:

$$\mathcal{P}(d, z | R) = \frac{d(L, F_c)^2}{M_*(z)} \int_0^{2\pi} d\phi \int_0^1 \mu \Sigma_*(q, z) d\mu$$

$$q = \sqrt{R^2 + r'^2 + 2dR\mu \cos(\phi)}$$

$$r' \equiv \mu d \quad \text{with} \quad 0 \leq \mu \leq 1$$

3. Model assumptions

For GRBs and SNe it is customary to factorize $\xi(L, z) = \phi(L)\psi(z)$, where $\phi(L)$ describes the luminosity distribution of

the event rate at $z = 0$, while the dimensionless function $\psi(z)$ is its redshifts evolution.

3.1. Luminosity function

We assume a broken power law $\phi(L)$ for long GRBs (Wanderman & Piran 2010; Salvaterra et al. 2012; Pescalli et al. 2016) as well as for short GRBs (Guetta & Piran 2005; Wanderman & Piran 2010; D’Avanzo et al. 2014; Ghirlanda et al. 2016) defined between L_{\min} and L_{\max} :

$$\phi(L) = n_0 \begin{cases} \left(\frac{L}{L_b}\right)^{-\alpha} & \text{if } L_{\min} < L < L_b \\ \left(\frac{L}{L_b}\right)^{-\beta} & \text{if } L_b < L < L_{\max} \end{cases} \quad (6)$$

where n_0 is the today (i.e., $z = 0$) rate at break luminosity L_b . GRBs are jetted sources, thus only the GRB jets pointing at the planet can be harmful. Here n_0 is the observed (not collimation corrected) rate an L the isotropic equivalent luminosity. n_0 is the ratio between ρ (i.e., cosmological rate at $z=0$, Table 1) and the integral of $\phi(L)$ with unit normalization. We assume that LGRBs and SGRBs have a distribution of characteristic duration centered around τ of 20s and 2s respectively (Kouveliotou et al. 1993). The energy (necessary to calculate the fluence) is derived from the luminosity L assuming that the burst with a duration τ has a triangular shape. This is fairly good approximation for SGRBs while it is an oversimplification of the complexity of LGRBs light curves. For long and short GRBs we adopt the parameter values reported in Table 1.

Concerning SNe, we consider the cosmic rate at $z = 0$ derived by Maoz & Mannucci (2012) and Li et al. (2011). The distribution of energy output of SNe can be described as gaussians (Hatano et al. 1997; Cappellaro et al. 1999; Richardson et al. 2002; Barris et al. 2004; Botticella et al. 2008; Yasuda & Fukugita 2010) with parameter values reported in Table 2. We further distinguish between the three different classes of SNe Ia, Ib and IIp.

3.2. Redshift distribution

The association of long GRBs with envelope stripped SNe (Galama et al. 1998; Stanek 2003; Hjorth et al. 2003; Malesani et al. 2005; Pian et al. 2006; Campana et al. 2006; Sparre et al. 2011; Melandri et al. 2012; Xu et al. 2013) and the properties of their hosts (e.g., Fruchter et al. 2006) probe their origin from the core-collapse of rapidly rotating massive stars (Woosley 1993; MacFadyen & Woosley 1999).

Being generated by the explosion of short lived massive stars, the redshift distribution of LGRBs and SNIbc/IIp should follow the cosmic star formation history (CSFR - e.g. Madau & Dickinson (2014); Hopkins & Beacom (2006)):

$$\psi_*(z) = 0.015 \frac{(1+z)^{2.7}}{1 + [(1+z)/2.9]^{5.6}} \text{ M}_{\odot} \text{yr}^{-1} \text{Mpc}^{-3} \quad (7)$$

represented by the blue line in Fig. 2. However, differently from SNIbc/IIp, the rate of long GRBs deviates from the CSFR (Firmani et al. 2004; Daigne et al. 2006; Le Floch et al. 2006; Guetta & Della Valle 2007; Kistler et al. 2009; Virgili et al. 2011; Salvaterra et al. 2012). This corresponds to a steeper (wrt the CSFR) increase of the GRB rate with increasing redshift (Pescalli et al. 2016) up to a peak corresponding to $z \sim 3.5$ (i.e. larger than the CSFR peak at $z \sim 2$). This could be interpreted as due to the GRB “bias” (i.e. preference) for low metallicity progenitors

	ρ [Gpc ⁻³ yr ⁻¹]	α	β	L_b [ergs s ⁻¹]	L_{min} [ergs s ⁻¹]	L_{max} [ergs s ⁻¹]	τ [s]
LGRB	1.3 ± 0.6	1.2 ± 0.9	2.4 ± 0.77	$10^{52.5 \pm 0.2}$	10^{49}	10^{54}	20
SGRB	0.3 ± 0.06	0.53 ± 0.88	3.4 ± 2.2	$(2.8 \pm 2.1) \times 10^{52}$	5×10^{49}	10^{53}	2

Table 1. Parameters of the LGRBs and SGRBs broken power law luminosity function (Wanderman & Piran 2010; Ghirlanda et al. 2016) and burst durations. ρ is the cosmological rate at $z = 0$.

(Woosley & Heger 2006). Hosts metallicity studies suggest that in most cases GRBs happen in galaxies with metallicity Z lower than a threshold value $\sim 0.7 Z_{\odot}$ (Vergani 2018; Palmerio et al. 2019). Population studies (Bignone et al. 2017, 2018) suggest that this metallicity threshold should be in the range $0.3\text{--}0.6 Z_{\odot}$. Assuming a threshold value $Z_c = 0.4 Z_{\odot}$ (Bertelli et al. 1994; Virgili et al. 2011) we therefore model the Long GRB population under this hypothesis and express their cosmic rate (orange line in Fig. 2) as:

$$\psi_{\text{LGRB}}(z) = \frac{\psi_{\star}(z)}{\psi_{\star}(0)} \frac{\Theta_{Z < Z_c}(z)}{\Theta_{Z < Z_c}(0)} \text{yr}^{-1} \text{Gpc}^{-3} \quad (8)$$

where $\Theta_{Z < Z_c}(z)$ is the fraction of stars with metallicity smaller than Z_c . We calculate $\Theta_{Z < Z_c}(0)$ by assuming that the metallicity of the local Universe has a mean value $[\text{Fe}/\text{H}]_0 = -0.006$ with a normal dispersion $\sigma = 0.22$ (Gallazzi et al. 2008; Madau & Dickinson 2014). As we will show in §3.4, the final rate of long GRBs within the MW does not depend on $\Theta_{Z < Z_c}(z)$ but only on its value at $z=0$.

Short GRBs are thought to be produced by the mergers of compact objects, as recently proved by the multimessenger observations of the event GW/GRB170817 (Abbott et al. 2017a,b). It is expected that their redshift distribution does not directly follow the CSFR due to the delay between their formation as a binary and their merger. The delay time distribution is a power law with slope -1 between few Myr and few Gyr (Guetta & Piran 2005; Nakar & Gal-Yam 2005; Guetta & Piran 2006; Wanderman & Piran 2015; Virgili et al. 2011). Ghirlanda et al. (2016) derived the SGRB formation rate from available observational constraints and found that, indeed, it is consistent with a delayed cosmic SFR history. We here adopt the parametric function obtained by their work (green line in Fig. 2):

$$\psi_{\text{SGRB}}(z) = \frac{1 + 2.8z}{1 + (z/2.3)^{3.5}} \text{yr}^{-1} \text{Gpc}^{-3} \quad (9)$$

For SNIa we assume the redshift distribution derived by Maoz & Mannucci (2012). This function is derived by convolving the star formation history of Hopkins & Beacom (2006) with a power law delay time distribution (DDT $\sim t^{-1}$). This DDT, in addition to ensuring an excellent fit to the observed SN rates, supports the hypothesis of a double-degenerate progenitor origin (i.e. merger of two WDs) for SNe Ia (Webbink 1984). The SNIa rate is shown by the red line in Fig. 2.

The cosmic rates of the three classes of transients considered in this work are compared in Fig. 2. $\psi_{\text{SGRB}}(z)$ and $\psi_{\text{SNIa}}(z)$ peak at a lower redshift compared to $\psi_{\star}(z)$ due to delay between their formation as a binary and their merger. $\psi_{\text{LGRB}}(z)$ peaks at higher redshift due to the metallicity bias.

3.3. Star formation factor

In order to account for the preference of LGRBs and core collapse SNe (Ibc/Iip, CCSNe) to occur in regions characterized by

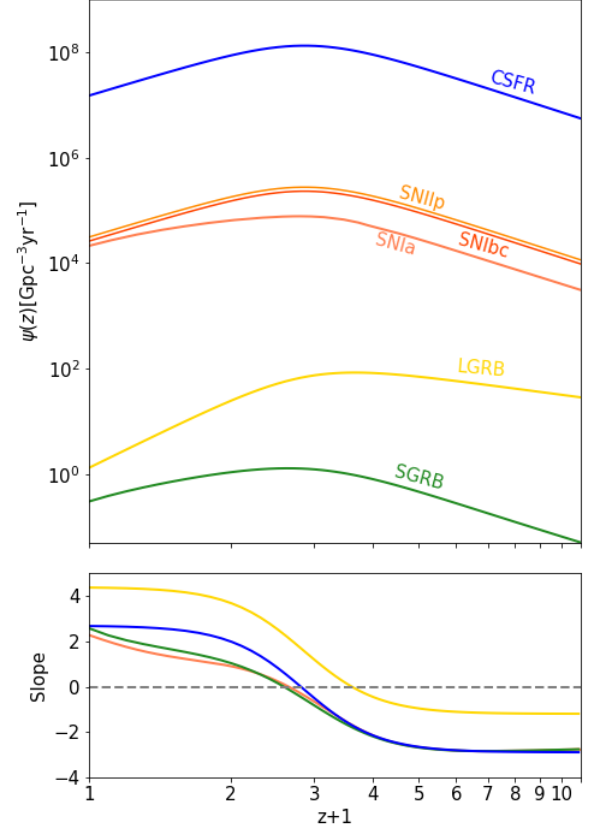


Fig. 2. *Top panel:* cosmic density rate of the 3 classes of high energy transients considered: LGRBs (yellow line), SGRBs (green line), SNe (orange lines). LGRB and SGRB rates are not corrected for the collimation angle, i.e. they represent the fraction of bursts whose jets are pointed towards the Earth. The CSFR (blue line) is in unit of $M_{\odot} \text{yr}^{-1} \text{Gpc}^{-3}$. All the curves are normalised to their respective local rate (see Table 1 and Table 2 for GRBs and SNe respectively). *Bottom panel:* derivative of the formation rate curves shown in the top panel. Same color coding. The derivative of SNIbc, Iip coincides with that of the CSFR (blue line in the bottom panel). The horizontal line identifies, for each curve the redshift z corresponding to the maximum of the rate curve.

a high star formation rate, we define (similarly to Li & Zhang 2015) the specific SFR correction factor:

$$f_{\text{sSFR}}(R, z) = \frac{s\text{SFR}(R, z)}{s\text{SFR}(z)} \quad (10)$$

that describes the fraction of the specific star formation within the MW, $s\text{SFR}(R, z)$, with respect to the specific cosmic star formation rate of the Universe at the same epoch $s\text{SFR}(z)$. $s\text{SFR}(R, z)$ is estimated (§3.5) through a model (Naab & Ostriker 2006, 2009) which describes the evolution of the radial profile of the star formation and stellar surface density of the MW. The local cosmic specific star formation rate $s\text{SFR}(z)$ is

defined as the ratio between the local star formation rate $\psi_*(z)$ (Madau & Dickinson 2014) and the average stellar density as a function of redshift $\rho_*(z) = 10^{17.46-0.39z} \text{ M}_\odot \text{ Gpc}^{-3}$ (Li & Zhang 2015; Mortlock et al. 2015). Note that, as expected, when we combine eq. 8 and eq. 10, the terms $\psi_*(z)$ cancels out (i.e., the global cosmological evolution of the star formation rate is irrelevant when we consider a specific galaxy), only the present day value $\psi_*(0)$ counts as a normalization factor.

3.4. Metallicity factor

In order to account for the preference of LGRBs to occur in low-metallicity environments, we define the correction factor:

$$f_{\text{Fe}}(R, z) = \frac{\Theta_{Z < Z_c}(R, z)}{\Theta_{Z < Z_c}(z)} \quad (11)$$

as the fraction of stars with metallicity smaller than $Z_c = 0.4Z_\odot$ (at any R and t) in the MW divided by the fraction of stars, with the same metallicity threshold, in the local Universe. This definition is similar to what adopted by Li & Zhang (2015), but we consider for the first time the metallicity profile and its time evolution within the MW.

As explained in §3.2, $\Theta_{Z < Z_c}(z)$ is elided with the same term in Eq. 8. Eq. 5 becomes:

$$\mathcal{P}(d, z | R) = \frac{1}{M_*(z)} \int_S \Sigma_*(R, z) f_{\text{SFR}}(R, z) f_{\text{Fe}}(R, z) da \quad (12)$$

The progenitor difference of SGRBs and LGRBs accounts for the preference of LGRBs to reside in high star formation and low-metallicity environments. Instead, there is no evidence of short GRBs preference for high star formation and low-metallicity environments. For this reason we assume $f_{\text{SFR,SGRB}} = 1$ and $f_{\text{Fe,SSGRB}} = 1$. The same holds for SNIa. For CCSNe we assume $f_{\text{SFR,CCSN}}$ as calculated in Eq. 10 and $f_{\text{Fe,CCSN}} = 1$ because for a progenitor with a mass $\leq 40 \text{ M}_\odot$ the formation of a SN is metallicity-independent (Heger et al. 2003). The rare case of SNe originated by a progenitor with mass $\geq 40 \text{ M}_\odot$ does not change significantly our results.

In order to account for the errors on the parameters of the luminosity functions, for the distribution of GRBs durations, SNe energies and rate, we implement a Monte Carlo simulation with 1000 realization for each type of lethal event. We calculate the number of lethal events during a time interval of 500 Myrs as the median value of the distribution of realizations. For each simulation we extract ρ , α , β , E_{SN} , L_b , and τ . For the first four parameters we assume they follow gaussian distributions with characteristic values as reported in Table 1 and Table 2. For L_b and τ we sample a log-normal distribution with characteristic values as reported in Table 1 and 2.

3.5. Galaxy model

To track the evolution and distribution of stellar surface density, star formation rate and metallicity of the Milky Way we use the inside-out formation model of Naab & Ostriker (2009). The model reproduces several observed properties of the present time Galaxy (Table 3).

They assume that the formation and evolution of MW proceeds in two phases. During the first phase (i.e. for cosmic time $t < 2.5 \text{ Gyr}$), the galaxy is coupled to the hierarchical growth of

SN type	Rate ($z=0$) $10^4 \text{ Gpc}^{-3} \text{ yr}^{-1}$	Burst Energy [erg]
Ia	2.2 ± 0.3 [a]	$10^{46 \pm 1}$ [c]
Ibc	2.6 ± 0.4 [b]	$10^{46 \pm 1}$ [c]
Iip	3.1 ± 0.5 [b]	$10^{44 \pm 1}$ [d]

Table 2. Parameters for the populations of SNe: cosmic rate and released energy (E_{SN}) for each SN type, as reported by Melott & Thomas (2011). [a] Maoz & Mannucci (2012), [b] Li et al. (2011), [c] Höflich & Schaefer (2009), [d] Soderberg et al. (2008), [e] Schawinski et al. (2008).

Propriety	Value
M_*	$5 \times 10^{10} \text{ M}_\odot$
M_{gas}	$1 \times 10^{10} \text{ M}_\odot$
$\Sigma_{*,\odot}$	$35 \text{ M}_\odot \text{ pc}^{-2}$
$\Sigma_{\text{gas},\odot}$	$15 \text{ M}_\odot \text{ pc}^{-2}$
SFR	$3 \text{ M}_\odot \text{ yr}^{-1}$

Table 3. Present-day Milky Way proprieties reproduced by model: total mass in stars, total mass in gas, stellar surface density at the solar radius, gas surface density at the solar radius, global star formation rate.

the large scale structure and the bulge is formed. After this initial phase, the dark matter halo evolves in isolation and the disk forms. In the absence of star formation, the bulge and the disk have an exponential surface density:

$$\Sigma_{\text{gas}}(R, z) = \Sigma_0(z) \exp[-R/R_s(z)] \quad (13)$$

where $\Sigma_0(z)$ and $R_s(z)$ are the central surface density and the scale length respectively. After bulge and gaseous disk formation, stars start to form following the local dynamical star formation model (Kennicutt 1998):

$$\Sigma_{\text{SFR}}(R, z) = \epsilon \frac{\Sigma_{\text{gas}}(R, z)}{\tau(R, z)} \quad (14)$$

where $\epsilon = 0.1$ represents the star formation efficiency and $\tau(R, z) = 2\pi R/v(z)$ is the orbital period of the disk of velocity $v(z)$.

In order to compute the surface stellar density $\Sigma_*(R, z)$ and metallicity $Z(R, z)$ distributions, Naab & Ostriker (2006, 2009) adopt a version of the chemical evolution (Ostriker & Tinsley 1975), which does not account for the radial gas flows. This model of the chemical evolution considers the instantaneous injection from massive stars and the delayed injection from low mass stars (see Naab & Ostriker 2006 for details).

Fig.3 shows the surface density star formation rate as a function of the position within the Galaxy (i.e. galactocentric radius R) vs. lookback-time. The density contours clearly show the increase of the star formation rate surface density from the inner part of the Galaxy towards the peripheral regions (*inside-out star formation*): while the innermost part of the Galaxy show little evolution of the star formation over time, the outskirts experienced an increase of several order of magnitudes.

Fig. 4 shows the evolution over cosmic time of the radial profile of the metallicity (in logarithmic scale - left color bar). Consistently with the increase of the star formation in the MW outskirts, also the metallicity at larger distances from the Galaxy center increased over the last Gyrs.

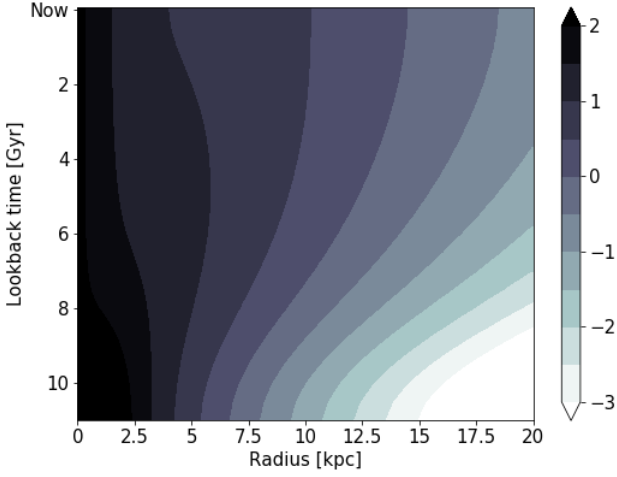


Fig. 3. Star formation surface density as a function of the galactocentric radius R and lookback time. Color coding (left color bar) is in logarithmic scale and in units of $M_{\odot}\text{pc}^{-2}\text{Gyr}^{-1}$.

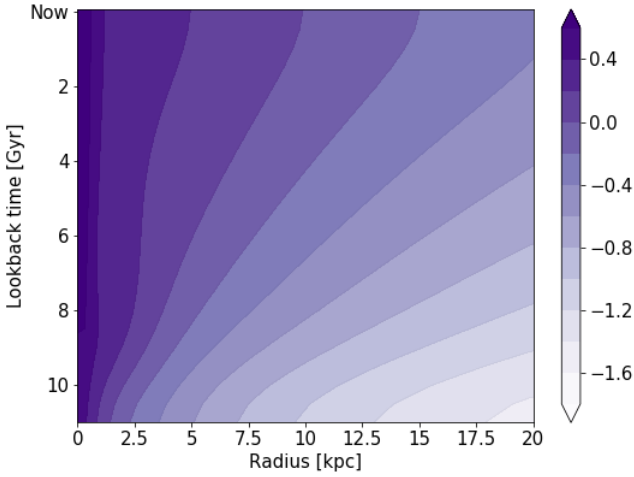


Fig. 4. Metallicity as a function of the galactocentric radius R and lookback time. The shaded regions (left color code) represent in logarithmic scale Z/Z_{\odot} .

3.6. Planetary formation

A terrestrial planet (TPs) is typically defined for having a solid-surface with radius and mass respectively in the ranges $0.5 - 2.0R_{\oplus}$ and $0.5 - 10M_{\oplus}$ (where R_{\oplus} and M_{\oplus} are the Earth radius and mass respectively). TPs could potentially develop habitable conditions (Alibert 2014). In order to estimate the surface number density of terrestrial planets (TPs) within the MW as a function of cosmic time and galactocentric distance, we adopt the model of Zackrisson et al. (2016). As simulations and observations (radial velocity and transit surveys) suggest, close-orbit giants (Hot Jupiters, HJ) form in metal-enriched environments, while in very low-metallicity environment planet formation is inhibited. The model, based on the assumption that HJs inhibit the formation of TPs, provides us that the probabilities of forming TP (P_{FTP}) and HJ (P_{FG}) as a function of the environment metallicity. Following Lineweaver et al. (2004) the probability for a star of harboring a TP is defined as:

$$P_{\text{HTP}} = P_{\text{FTP}}(1 - P_{\text{FG}}) \quad (15)$$

Zackrisson et al. (2016) approximates the probability of forming HJ as a function of the metallicity $[Fe/H]$ and of the stellar mass M_{\star} (Gaidos & Mann 2014):

$$P_{\text{FG}}([Fe/H], M_{\star}) = f_0 10^{a[Fe/H]} M_{\star}^b \quad (16)$$

where $f_0 = 0.07$ is a constant factor and the parameter values are $a = 1.8(1.06)$ for FGK (M) stars and $b = 1$ (Gaidos & Mann 2014). The probability of forming terrestrial planets is (Zackrisson et al. 2016):

$$P_{\text{FTP}} = f_{\text{TP}} k(Z) \quad (17)$$

with $f_{\text{TP}} = 0.4(1)$ for FGK (M) stars. $k(Z)$ is a function with a cut-off at low-metallicity values:

$$k(Z) = \begin{cases} 0 & \text{if } [Fe/H] \leq -2.2 \\ \frac{Z-0.001}{0.001-0.0001} & \text{if } -2.2 \leq [Fe/H] \leq -1.2 \\ 1 & \text{if } [Fe/H] \geq -1.2 \end{cases}$$

Combining these equations with the Galaxy model of Naab & Ostriker (2009) (§3.5) we can compute $P_{\text{HTP}}(R, t)$ accounting for the metallicity radial distribution and its cosmic evolution within the Galaxy. The number surface density of TPs as function of time along MW is computed using the star formation surface density derived in §3.5 and assuming a Salpeter initial mass function: we compute the fraction of M dwarfs f_{M} (with masses in the range $0.1-0.6 M_{\odot}$) and FGK stars f_{FGK} (with masses in the range $0.6-1.2 M_{\odot}$). Assuming an average mass for M stars of $0.35 M_{\odot}$ and $0.9 M_{\odot}$ for FGK stars we derive the number surface density of TPs around M dwarfs and FGK stars with the following equation:

$$\Sigma_{\text{TP}}(R, z) = \int_{z_{\text{form}}}^z \frac{f \Sigma_{\text{SFR}}(R, z) P_{\text{HTP}}(R, t)}{\langle M \rangle} dz \quad (18)$$

where $z_{\text{form}} = 2.5$ is the formation redshift of the MW in the model of Naab & Ostriker (2009).

4. Results

Figure 5 shows the number of lethal astrophysical transient events (red solid line) in the last 500 Myr as a function of distance from Galactic Center. The yellow solid line in Fig. 5 shows the number of lethal LGRBs, while the orange solid line and the green solid line denotes the number of lethal SNe and SGRBs, respectively. In Fig. 5 we also show (referred to the left vertical axis) the surface number density of Terrestrial Planets (TPs) around M stars (dark blue dashed line) and around FGK stars (light blue dashed line). At the Earth's position (8 kpc – vertical black solid line), the number of lethal events (predominantly LGRBs) is $\sim 1-2$ within the last 500 Myr. This agrees with the hypothesis ascribing the Ordovician mass extinction event to a LGRB (Melott et al. 2005). There is a minimum in the red solid line (i.e. LGRBs+SGRBs+SNe) which identifies a region between ~ 2 and ~ 8 kpc from the Galaxy Center where life, in the last 500 Myrs, could have suffered ≤ 1 lethal events. In the outskirts ($R > 10$ kpc) and in the center ($R < 1.5$ kpc) of the MW the number of lethal event is > 2 . In the outskirts of the Galaxy, due to low metallicity environment, predominant lethal events are LGRBs, while in the star forming environment of the Center, SGRs and SNe predominantly occur. The outskirts of the MW are not favoured for hosting life due to the low density of TPs (dashed lines) and the high frequency of lethal LGRBs.

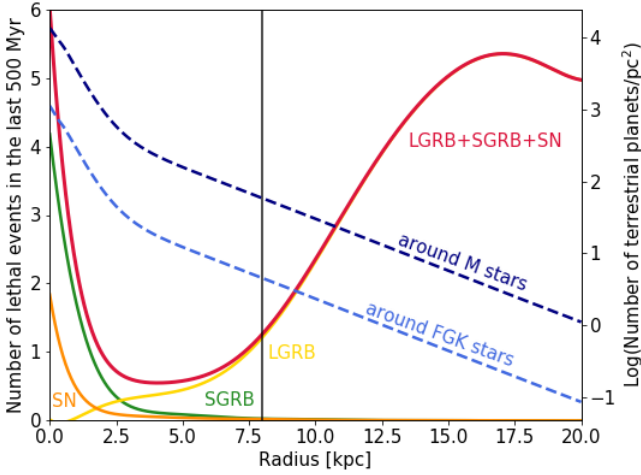


Fig. 5. Number of lethal astrophysical transient events (solid red line) in the last 500 Myr as a function of distance from the Galactic Center. The individual contributions of Short GRBs (SGRBs – green solid line), Long GRBs (LGRBs – yellow solid line) and Supernovae (SNe – orange solid line) are shown. The surface number density of Terrestrial Planets (TPs) around M stars (dark blue dashed line) and around FGK stars (light blue dashed line) are reported (referred to the left hand side vertical axis). The vertical black solid line at 8 kpc marks the solar system position where the total number of lethal events (predominantly LGRBs) is ~ 1.3 .

Figure 6 shows the number of lethal events (SGRBs+LGRBs+SNe, shaded contours corresponding to the green–yellow–red color bar) per bins of time of 500 Myr as a function of the distance from the Galactic Center (x-axis) along Milky Way cosmic history (y-axis). The line contours (corresponding to the blue-scale color bar) show the surface number density of terrestrial planets around M stars (solid lines) and FGK stars (dashed lines).

The individual contributions of SGRBs and LGRBs to Fig. 6 are shown in Fig. 7 and Fig. 8. Short GRBs (Fig. 8) are concentrated in the central regions of the Galaxy due to the large stellar density and their occurrence being independent from the metallicity of the environment. On the other hand, the incidence of long GRBs as lethal events (Fig. 7) develops along the MW history with an inside–out pattern: they dominate the rate of lethal events in the early stages of the MW evolution in the central regions, where most of the stars are formed, but are progressively suppressed due to the increase of the metallicity and they become more prominent towards the outskirts where the star formation is relatively higher and the metal pollution yet not dramatic.

There are two “green valleys” along the MW disk and its cosmic history. The first “green valley” is the outer regions of the disk (i.e. $R > 12$ kpc) which suffered a relatively low incidence of lethal events during the first 6 Gyrs of the Galaxy evolution. This region, however, has the lowest TP surface density. Starting around 6 Gyrs ago, owing to their energetics, long GRBs became the dominant lethal sources for life within the MW, with an increasing number of lethal events towards the Galaxy periphery (red-to-orange contours in Fig. 1). This is due to the increased conversion rate of relatively low metal polluted gas into massive stars in the outer regions of the MW. Such global trend determined the formation of an increasingly larger, safer region of the MW located at intermediate galactocentric distances $R \in (2 - 8)$ kpc. In this second “green valleys” the main contribution of lethal events is still due to LGRBs but the increase of the metal-

	$0.3 Z_{\odot}$	$0.4 Z_{\odot}$	$0.5 Z_{\odot}$
8 kpc	1.5	1.2	1.0
17 kpc	2.9	5.3	7.4

Table 4. Number of lethal LGRBs at 8 kpc and at 17 kpc in the last 500 Myrs considering different metallicity threshold

licity due to the intense star formation suppresses the incidence of LGRBs. The higher density of TPs in this region makes it the most favourable region of the Galaxy for the development and resilience of life to ozone depletion induced by transient astrophysical events over the last 4 Gyrs. In general, the early stages of the MW evolution (from its formation up to 6 billion years ago) witnessed extremely bad conditions for life development due the presence of lethal events over almost all the Galactic disk ($R < 10 - 12$ kpc) where TPs are present in a considerable number.

5. Discussion and Conclusions

In this work, we investigate the impact of the most energetic transient events on planetary habitability inside the MW and along its cosmic history. We consider Long GRBs, Short GRBs and SNe (Ia, Ib and IIp). These are the most energetic transients which can illuminate a planet atmosphere with a gamma-ray fluence $> 100 \text{ kJ m}^{-2}$ (10^8 erg cm^{-2}).

This fluence threshold is considered harmful for life because it would induce a 90% depletion of the ozone layer, i.e. a change able to trigger a mass extinction (Thomas et al. 2005a). The choice of the threshold value impacts on the estimate of the rate of lethal events but not on their spatial and temporal trends within the MW. If we consider a smaller threshold fluence of 10 kJ m^{-2} (able to induce a 68% depletion of the ozone layer) there would be lethal events at larger distances which would increase the total rate at any R and at any time. On the contrary, a larger threshold fluence of 1000 kJ m^{-2} (98% depletion of the ozone layer) would select only the most powerful transients exploding closer to any planet. These events are relatively rare given the corresponding steep luminosity function of LGRBs and SGRBs. Notice that the threshold adopted in this work, i.e. $> 100 \text{ kJ m}^{-2}$ (10^8 erg cm^{-2}), is larger than the lethal dose typically considered for Earth biota which is 10^5 erg cm^{-2} for eucaryotic multicellular lifeforms (Scalo & Wheeler 2002) and 10^7 erg cm^{-2} for prokaryotic microbes (Balbi & Tombesi 2017). This allows us to extend our results also to planets without an ozone layer.

The lethal effect of the three classes of transients is evaluated considering their energetics and rates combined with the surface density of terrestrial planets. We find that LGRBs are the dominant life-threatening transients for planets at $R > 2$ kpc along the entire MW cosmic history (Fig. 7). This is mainly due to their large energy 10^{51-54} ergs (isotropic equivalent) which compensates, compared to SNe, for their lower intrinsic rate. While SGRBs compete with long ones in terms of energetic and rate, their occurrence is mainly driven by the star formation rate thus dominating the central regions of the MW and, in particular, during the earliest epochs of the MW evolution (Fig. 8).

We link both LGRB and the TP formation rate to the metallicity evolution within the MW. We consider that LGRBs preferably form in environments with $Z < 0.4 Z_{\odot}$ (Bignone et al. 2017, 2018). Assuming a different metallicity threshold value (Tab. 4), mainly affects the rate of lethal LGRBs in the outer regions of the Galaxy, where the metallicity is close to this threshold value.

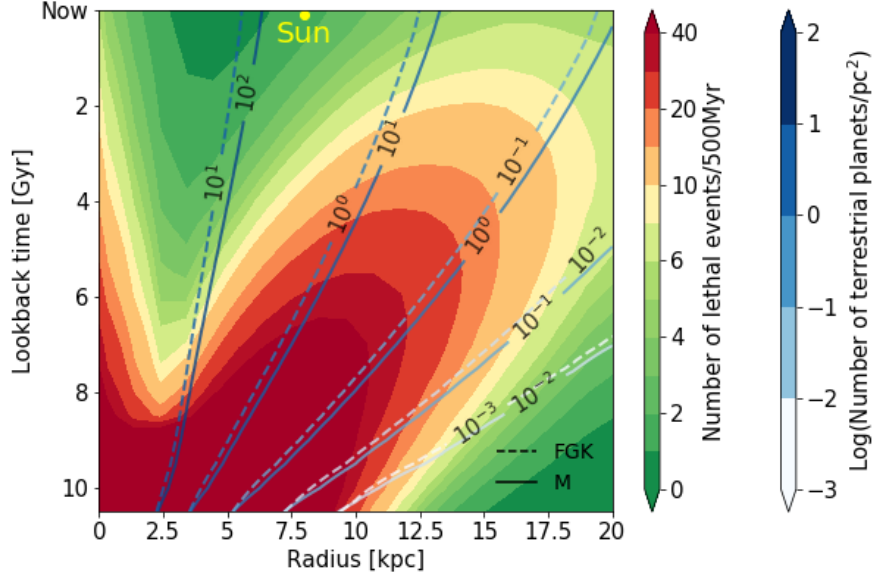


Fig. 6. Shaded contours (corresponding to the green–yellow–red color bar) show the number of lethal events (SSGRBs+LGRBs+SNs) per 500 Myr as a function of the distance from the Galactic Center (x-axis) along Milky Way cosmic history (y-axis). The line contours (corresponding to the blue-scale color bar) show the surface number density of terrestrial planets around M stars (solid lines) and FGK stars (dashed lines). The present position of the solar system is marked by the yellow dot. The Galaxy disk portion comprised between ~ 2 and ~ 8 kpc from the Galaxy center, where there is a relatively larger terrestrial planet density, represent the place where life, in the last 4 Gyrs, could have suffered less frequently major damages due to ozone depletion induced by transient astrophysical events.

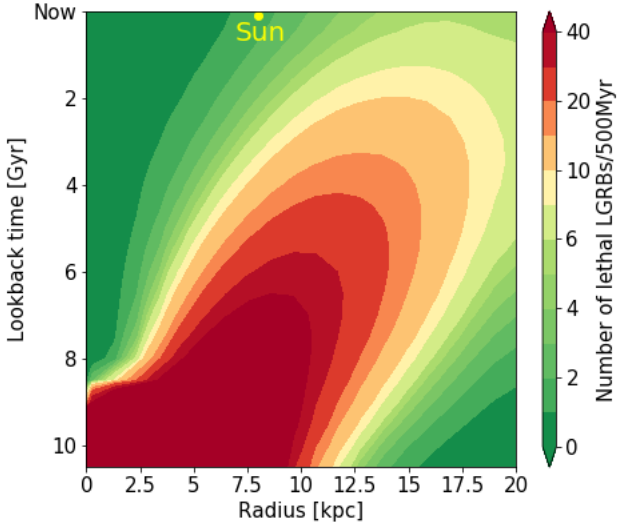


Fig. 7. Number of lethal long GRBs per bins of 500 Myr as a function of the galactic radius and lookback time.

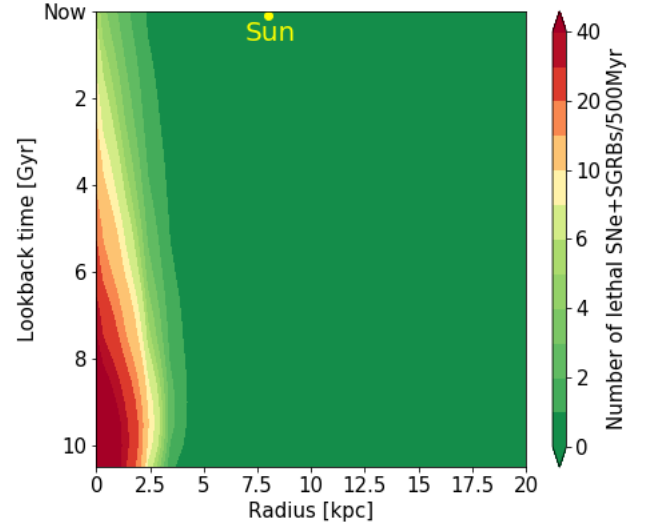


Fig. 8. Number of lethal short GRBs and SNe per bins of 500 Myr as a function of the galactic radius and lookback time.

The lethal impact of SGRB, which dominate the central regions of the Galaxy (Fig.8), has been computed assuming the luminosity function derived by Ghirlanda et al. (2016). If, alternatively, we consider a steeper faint end of the SGRB luminosity function (as derived in Wanderman & Piran 2015, only the rate of low luminosity SGRBs would result increased. These events are characterized by relatively small hazard distances (Eq. 4) due to their low luminosity and our results would be practically unaltered.

In our analysis we have not considered other aspects which are investigated by recent works in the context of galactic habitability. For example, the combined action of tidal disruption events (Pacetti et al. 2020) and the active phase of the central black hole (Balbi & Tombesi 2017) further reduce the habitability of the bulge. Moreover, a proper evaluation of the habitability of the bulge should also account for the relatively higher probability of stellar encounters which can perturb planetary orbital configuration but, on the other hand, also favor lithopanspermia (Melosh 1988; Wesson 2010).

As suggested by O'Neill et al. (2020), planets forming early on in the MW history tend to have low Fe/Si ratios and thus strong plate tectonic activity which seems to be an important factor for the development of life as we know it. However, as emerging in our work, during the early stages of the Galaxy, these planets were subject to a very high rate of lethal events.

In a recent work, Marshall et al. (2020) suggest that the moderate extinction event at the end of the Devonian period (Hangenberg event, ~ 360 Myrs) was associated with ozone depletion and a consequent larger Sun UV-B radiation reaching the Earth. This may explain the discovery of malformed land plant spores in terrestrial Devonian-Carboniferous boundary sections from East Greenland. Although a GRB cannot be excluded as the cause of this extinction event, Fields et al. 2020 propose cosmic rays, accelerated in a nearby supernova and magnetically confined inside the SN remnant for ~ 100 kyrs, as trigger of the ozone layer depletion and thus the late Devonian extinctions. In our work we did not take into account the effect of cosmic rays.

Our main results can be summarized as follows:

- we confirm that at the Earth position, within the last 500 Myr, one long GRB may have occurred thus having a leading role in the Ordovician mass extinction;
- the safest zone in the last 500 Myr is around 2-8 kpc. Differently from what has been claimed by recent works, we find that the outskirts are not favoured for hosting life. This is due to the low density of TPs (dashed lines in Fig.5) and the high frequency of lethal LGRBs, which hinders the emergence of a long-lasting biosphere. Short GRBs and SNe are the dominant lethal events only in the central regions of the Galaxy. Search for exoplanets harbouring lifeforms should have more chances of success looking in the direction of the Galactic center, within 5 kpc from the Sun, due to combined effect of high density of terrestrial planets (dashed line in Fig.5) and of low occurrence of lethal transients (solid red line in Fig.5);
- we identify two “green valleys” along the MW disk and its cosmic history (Fig.6). The first “green valley” is located in the outskirts of the galactic disk (i.e. $R > 12$ kpc). These regions suffered a relatively low incidence of lethal events during the first 6 Gyrs of the Galaxy evolution. However, the chances of life emergence is hampered by the low TP surface density. The other “green valley” is located at intermediate galactocentric distances $R \in (2 - 8)$ kpc. Here the dominant lethal transients were LGRBs until 7-6 Gyrs but, later on, the progressive increase of the metallicity due to the intense star formation suppressed the lethal incidence of LGRBs. The higher density of TPs in this region makes it the most favourable place of the Galaxy for the resilience of life to mass extinction induced by transient astrophysical events over the last ~ 4 Gyrs.

In conclusion, most powerful cosmic explosion jeopardized life across most of the Milky Way in the past, not anymore. In particular, until ~ 6 Gyrs ago the entire Galaxy was very frequently sterilized by transient events. In the early stage of the Galaxy evolution, life as we know it should have been more resilient to high radiation irradiance in order to survive. If we exclude the “green valley” in the bottom-right side of Fig. 6 which has the lowest TP surface density, the Galaxy is overall a safer place to live on a planet today than in the past. If we assume that Sun did not significantly migrate along the galactocentric radius during its lifetime, the Earth, from its birth until today, experienced an ever lower rate of potential mass extinctions events and gradually became an increasingly safer place.

Finally, we note that the very existence of life on planet Earth today demonstrates that mass extinctions do not necessarily preclude the possibility of complex life development. On the contrary, mass extinctions happening at the “right pace” could have played a pivotal role in the evolution of complex lifeforms on our home planet (Sepkoski 1985; Raup 1994; Jablonski 2001; Krug & Jablonski 2012; Stroud & Losos 2016).

Acknowledgements. R.S. acknowledges the Brera Observatory for the kind hospitality during the completion of this work. The authors thank F. Borsa for useful discussions. Funding support is acknowledged from Prin-INAF 1.05.01.88.06 “Towards the SKA and CTA era: discovery, localisation, and physics of transient sources”; 1.05.06.13 Premiale 2015 “FIGARO”; Accordo Attuativo ASI-INAF n.2017-14-H.0.

References

- Abbott, B. P., Abbott, R., Abbott, T. D., et al. 2017, *Phys. Rev. Lett.*, 119, 161101
 Abbott, B. P., Abbott, R., Abbott, T. D., et al. 2017, *Phys. Rev. Lett.*, 119, 141101
 Alibert, Y. 2014, *A&A*, 561, A41
 Balbi, A. & Tombesi, F. 2017, *Scientific Reports*, 7, 16626
 Barris, B. J., Tonry, J. L., Blondin, S., et al. 2004, *ApJ*, 602, 571
 Bertelli, G., Bressan, A., Chiosi, C., et al. 1994, *A&AS*, 106, 275
 Bignone, L. A., Tissera, P. B., & Pellizza, L. J. 2017, *MNRAS*, 469, 4921
 Bignone, L. A., Pellizza, L. J., & Tissera, P. B. 2018, *New A*, 65, 73
 Botticella, M. T., Riello, M., Cappellaro, E., et al. 2008, *A&A*, 479, 49
 Campana, S., Mangano, V., Blustin, A. J., et al. 2006, *Nature*, 442, 1008
 Cappellaro, E., Evans, R., & Turatto, M. 1999, *A&A*, 351, 459
 Dar, A., Laor, A., & Shaviv, N. J. 1998, *Phys. Rev. Lett.*, 80, 5813
 Daigne, F., Rossi, E. M., & Mochkovitch, R. 2006, *MNRAS*, 372, 1034
 D’Avanzo, P., Salvaterra, R., Bernardini, M. G., et al. 2014, *MNRAS*, 442, 2342
 Fields, B. D., Melott, A. L., Ellis, J., et al. 2020, *arXiv:2007.01887*
 Firmani, C., Avila-Reese, V., Ghisellini, G., et al. 2004, *ApJ*, 611, 1033
 Fruchter, A. S., Levan, A. J., Strolger, L., et al. 2006, *Nature*, 441, 463
 Gaidos, E. & Mann, A. W. 2014, *ApJ*, 791, 54
 Galama, T. J., Vreeswijk, P. M., van Paradijs, J., et al. 1998, *Nature*, 395, 670
 Gallazzi, A., Brinchmann, J., Charlot, S., et al. 2008, *MNRAS*, 383, 1439
 Gehrels, N., Laird, C. M., Jackman, C. H., et al. 2003, *ApJ*, 585, 1169
 Ghirlanda, G., Salafia, O. S., Pescalli, A., et al. 2016, *A&A*, 594, A84
 Gowanlock, M. G., Patton, D. R., & McConnell, S. M. 2011, *Astrobiology*, 11, 855
 Gowanlock, M. G. 2016, *ApJ*, 832, 38
 Guetta, D. & Piran, T. 2005, *A&A*, 435, 421
 Guetta, D. & Piran, T. 2006, *A&A*, 453, 823
 Guetta, D. & Della Valle, M. 2007, *ApJ*, 657, L73
 Hatano, K., Fisher, A., & Branch, D. 1997, *MNRAS*, 290, 360
 Heger, A., Fryer, C. L., Woosley, S. E., et al. 2003, *ApJ*, 591, 288
 Herrmann, A. D., & Patzkowsky, M. E. (2002) *Astrobiology* 2, 560-561
 Herrmann, A. D., Patzkowsky, M. E., & Pollard, D. 2003, *Geology*, 31, 485
 Hjorth, J., Sollerman, J., Møller, P., et al. 2003, *Nature*, 423, 847
 Höflich, P. & Schaefer, B. E. 2009, *ApJ*, 705, 483
 Hopkins, A. M. & Beacom, J. F. 2006, *ApJ*, 651, 142
 Jablonski, D. 2001, *PNAS*, 98, 5393-5398
 Japelj, J., Vergani, S. D., Salvaterra, R., et al. 2016, *A&A*, 590, A129
 Kasting, J. F., Whitmire, D. P., & Reynolds, R. T. 1993, *Icarus*, 101, 108
 Kennicutt, R. C. 1998, *ApJ*, 498, 541
 Kistler, M. D., Yüksel, H., Beacom, J. F., et al. 2009, *ApJ*, 705, L104
 Kopparapu, R. K., Ramirez, R., Kasting, J. F., et al. 2013, *ApJ*, 765, 131
 Kouveliotou, C., Meegan, C. A., Fishman, G. J., et al. 1993, *ApJ*, 413, L101
 Krug, A. Z. & Jablonski, D. 2012, *Geology*, 40, 731
 Le Floc’h, E., Charmandaris, V., Forrest, W. J., et al. 2006, *ApJ*, 642, 636
 Li, Y. & Zhang, B. 2015, *ApJ*, 810, 41
 Li, W., Leaman, J., Chornock, R., et al. 2011, *MNRAS*, 412, 1441
 Lineweaver, C. H., Fenner, Y., & Gibson, B. K. 2004, *Science*, 303, 59
 MacFadyen, A. I. & Woosley, S. E. 1999, *ApJ*, 524, 262
 Madau, P. & Dickinson, M. 2014, *ARA&A*, 52, 415
 Malesani, D., Moretti, A., Romano, P., et al. 2005, *GRB Coordinates Network*, Circular Service, No. 3087, #1 (2005), 3087
 Maoz, D. & Mannucci, F. 2012, *PASA*, 29, 447
 Marshall, J. E. A., Lakin, J., Troth, I., et al. 2020, *Science Advances*, 6, eaba0768
 Melandri, A., Pian, E., Ferrero, P., et al. 2012, *A&A*, 547, A82
 Melosh, H. J. 1988, *Nature*, 332, 687
 Melott, A. L., Thomas, B. C., Hogan, D. P., et al. 2005, *Geophys. Res. Lett.*, 32, L14808
 Melott, A. L. & Thomas, B. C. 2011, *Astrobiology*, 11, 343
 Mortlock, A., Conselice, C. J., Hartley, W. G., et al. 2015, *MNRAS*, 447, 2
 Naab, T. & Ostriker, J. P. 2006, *MNRAS*, 366, 899

- Naab, T. & Ostriker, J. P. 2009, *ApJ*, 690, 1452
- Nakar, E. & Gal-Yam, A. 2005, American Astronomical Society Meeting Abstracts
- Ostriker, J. P. & Tinsley, B. M. 1975, *ApJ*, 201, L51
- O'Neill, C., Lowman, J., & Wasiliev, J. 2020, *Icarus*, 352, 114025
- Pacetti, E., Balbi, A., Lingam, M., et al. 2020, *MNRAS*, doi:10.1093/mnras/staa2535
- Palmerio, J. T., Vergani, S. D., Salvaterra, R., et al. 2019, *A&A*, 623, A26
- Pescalli, A., Ghirlanda, G., Salvaterra, R., et al. 2016, *A&A*, 587, A40
- Pian, E., Mazzali, P. A., Masetti, N., et al. 2006, *Nature*, 442, 1011
- Piran, T. & Jimenez, R. 2014, *Phys. Rev. Lett.*, 113, 231102
- Pescalli, A., Ghirlanda, G., Salvaterra, R., et al. 2016, *A&A*, 587, A40
- Raup, D.M. 1994, *PNAS*, 91, 6758-6763
- Ruderman, M. A. 1974, *Science*, 184, 1079
- Richardson, D., Branch, D., Casebeer, D., et al. 2002, *AJ*, 123, 745
- Salvaterra, R., Campana, S., Vergani, S. D., et al. 2012, *ApJ*, 749, 68
- Scalo, J. & Wheeler, J. C. 2002, *ApJ*, 566, 723
- Schawinski, K., Justham, S., Wolf, C., et al. 2008, *Science*, 321, 223
- Sepkoski, J. J. 1985, *The Search for Extraterrestrial Life: Recent Developments*, 112, 223
- Soderberg, A. M., Berger, E., Page, K. L., et al. 2008, *Nature*, 453, 469
- Sparre, M., Sollerman, J., Fynbo, J. P. U., et al. 2011, *ApJ*, 735, L24
- Spitoni, E., Matteucci, F., & Sozzetti, A. 2014, *MNRAS*, 440, 2588
- Stanek, M. J. 2003, *Acoustical Society of America Journal*, 113, 1788
- Stroud J.T. & Losos, J.N. 2016, *Annual Review of Ecology, Evolution, and Systematics*, 47, 507-532
- Svensmark, H. 2012, *MNRAS*, 423, 1234
- Thomas, B. C., Jackman, C. H., Melott, A. L., et al. 2005, *ApJ*, 622, L153
- Thomas, B. C., Melott, A. L., Jackman, C. H., et al. 2005, *ApJ*, 634, 509
- Thorsett, S. E. 1995, *ApJ*, 444, L53
- Vergani, S. D. 2018, *Mem. Soc. Astron. Italiana*, 89, 175
- Virgili, F. J., Zhang, B., Nagamine, K., et al. 2011, *MNRAS*, 417, 3025
- Vukotić, B., Steinhauser, D., Martinez-Aviles, G., et al. 2016, *MNRAS*, 459, 3512
- Wanderman, D. & Piran, T. 2010, *MNRAS*, 406, 1944
- Wanderman, D. & Piran, T. 2015, *MNRAS*, 448, 3026
- Webbink, R. F. 1984, *ApJ*, 277, 355
- Wesson, P. S. 2010, *Space Sci. Rev.*, 156, 239
- Woosley, S. E., Langer, N., & Weaver, T. A. 1993, *ApJ*, 411, 823
- Woosley, S. E. 1993, *ApJ*, 405, 273
- Woosley, S. E. & Heger, A. 2006, *ApJ*, 637, 914
- Xu, D., de Ugarte Postigo, A., Leloudas, G., et al. 2013, *ApJ*, 776, 98
- Yasuda, N. & Fukugita, M. 2010, *AJ*, 139, 39
- Yoon, S.-C., Langer, N., & Norman, C. 2006, *A&A*, 460, 199
- Zackrisson, E., Calissendorff, P., González, J., et al. 2016, *ApJ*, 833, 214